GEOLOGICAL SURVEY OF CANADA
COMMISSION GÉOLOGIQUE DU CANADA

PAPER 76-25

VLF MAPPING OF GEOLOGICAL STRUCTURE

W.M. TELFORD
W.F. KING
A. BECKER

Energy, Mines and Resources Canada
Énergie, Mines et Ressources Canada

1977

GEOLOGICAL SURVEY
PAPER 76-25

VLF MAPPING OF GEOLOGICAL STRUCTURE

W.M. TELFORD
W.F. KING
A. BECKER

1977

Printing and Publishing
Supply and Services Canada,
Ottawa, Canada K1A 0S9,

from the Geological Survey of Canada
601 Booth St., Ottawa, K1A 0E8

or through your bookseller.

Catalogue No. M44-76-25
ISBN - 0-660-00811-4

Price: Canada: $2.50
Other Countries: $3.00

Price subject to change without notice

CONTENTS

Illustrations

VLF MAPPING OF GEOLOGICAL STRUCTURE

Abstract

Field measurements with the EM16 instrument, in several areas definitely confirm the usefulness of the VLF method for mapping shallow geological structure. Results obtained across a portion of the Gloucester fault southeast of Ottawa indicate that this technique is particularly suitable in areas where the geology is simple. The field results generally agree rather well with theoretical model data. The latter, however, indicates that mapping with the EM16 alone produces little quantitative information, although the relative positions of the high and low resistivity beds are generally clear. For this reason, it is desirable to supplement the EM16 data occasionally with surface impedance measurements to obtain apparent resistivities on both sides of the contact. This is especially true where it is suspected that the observed anomaly is caused by an accident in the bedrock topography rather than by the opposition of beds of differing resistivity.

Résumé

Des mesures, sur terrain, avec l'appareil EM16 confirment l'utilité de la méthode TBF comme outil de cartographie des structures géologiques peu profondes. Les résultats obtenus à travers la faille de Gloucester au sud-ouest d'Ottawa indiquent que cette technique s'adapte très bien au problème posé dans des situations géologiquement simples.

Les résultats de terrain concordent très bien avec les calculs théoriques. Cependant ceux-ci démontrent qu'il est difficile d'obtenir des informations quantitatives à partir des mesures EM16 seules. Afin d'obtenir des résistivités apparentes des deux côtés du contact, on doit compléter les mesures EM16 avec des mesures de l'impédance de surface. Ceci est surtout vrai dans des cas où l'on soupçonne que l'anomalie est liée à un accident topographique de la roche en place plutôt que par une opposition des lits de résistivité différente.

VLF MAPPING OF GEOLOGICAL STRUCTURE

W.M. Telford[1], W.F. King[2] and A. Becker[3]

Foreword

This paper is a summary of the work done by W.F. King while working under the direction of Dr. A. Becker as a graduate assistant for the Geological Survey of Canada during the summers of 1969 and 1970. The data described form part of his M.Sc. Thesis dissertation, working under thesis supervisor, Prof. W.M. Telford, Department of Mining Engineering and Applied Geophysics, McGill University. This paper is a product of the application of new geophysical techniques being adapted to the geological mapping mission of the Electrical Methods Section, Resource Geophysics and Geochemistry Division, Geological Survey of Canada.

L.S. Collett,
Head, Terrain Geophysics Program,
Resource Geophysics and Geochemistry Division

INTRODUCTION

It has long been observed that electromagnetic plane waves propagating along the earth's surface are locally distorted by near-surface discontinuitites in electrical resistivity. In such cases the horizontal magnetic field components normally present induce in the ground a non-uniform eddy current distribution which results in an anomalous vertical magnetic field component. In the extra low frequency range (ELF) this phenomenon is readily observable near coastlines (Weaver, 1963) while in the audiofrequency range (AFMAG) the effect was first observed by Shaw (oral comm., 1961) in the vicinity of faults and shear zones. More recently, Collett and Bell (1971) have discussed how the AFMAG method can serve as a useful tool in structural mapping. Finally at very low frequencies (VLF) i.e. in the 10-20 kHz range the effect of geological structure has been observed by Becker (1967), Fraser (1969) and Patterson and Ronka (1971).

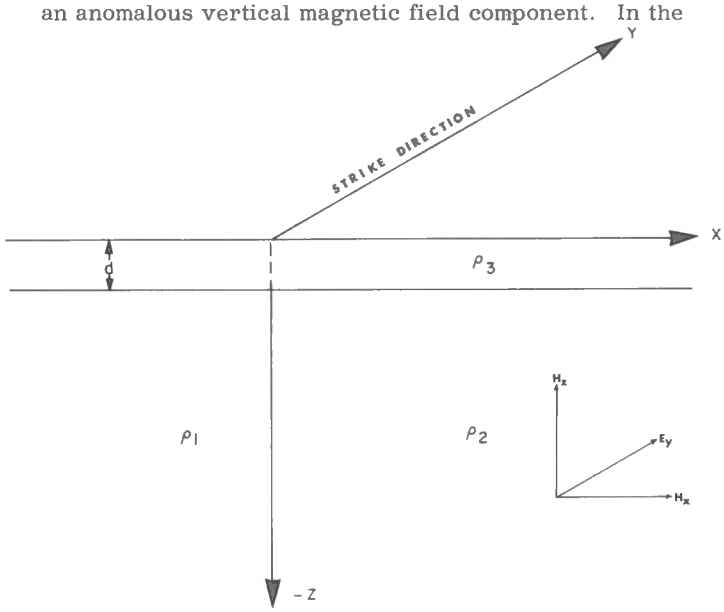

Figure 1. Two-dimensional fault with strike length infinite in y-direction: insert shows E polarization vectors.

These effects were explained theoretically by Weaver (1963) who obtained closed form solutions for plane waves incident on a semi-infinite conducting medium divided by a vertical discontinuity into two regions of different resistivity. Weaver's calculations were later confirmed experimentally by Dosso (1976) on a laboratory scale model. Both authors forecast a sharp increase in vertical magnetic field component near an electrical discontinuity. This quantity exhibits a maximum value at the discontinuity and decreases gradually to zero away from it.

The rate of decrease is a function of the electrical properties of the material on either side of the discontinuity, being greater on the conductive side. More recently this problem was studied by Geyer (1972a, b) who found that the spatial variation of the vertical component was strongly influenced by the dip of the interface.

The purpose of the present study was to examine in some detail the variation exhibited by the field components of a plane electromagnetic wave in the vicinity of a fault. In particular we have elected to study the variation in the vertical magnetic component and in the surface wave impedance across the discontinuity. As will be shown later, in the results section, we were fortunate to be able to perform the measurements in relatively simple geological environments so that a good comparison could be made between our theoretical predictions of electromagnetic field behaviour and the observed variations.

[1]Department of Geophysics, McGill University, P.O. Box 6070, Station A, Montreal H3C 3G1, Canada

[2]Chevron Standard Company Ltd., 400 5th Ave. S.W. Calgary, Alberta

[3]Managing Director, IREM-MERI, P.O Box 6079, Station A, Montreal H3C 3A7, Canada

Manuscript received and approved for publication, August, 1976.

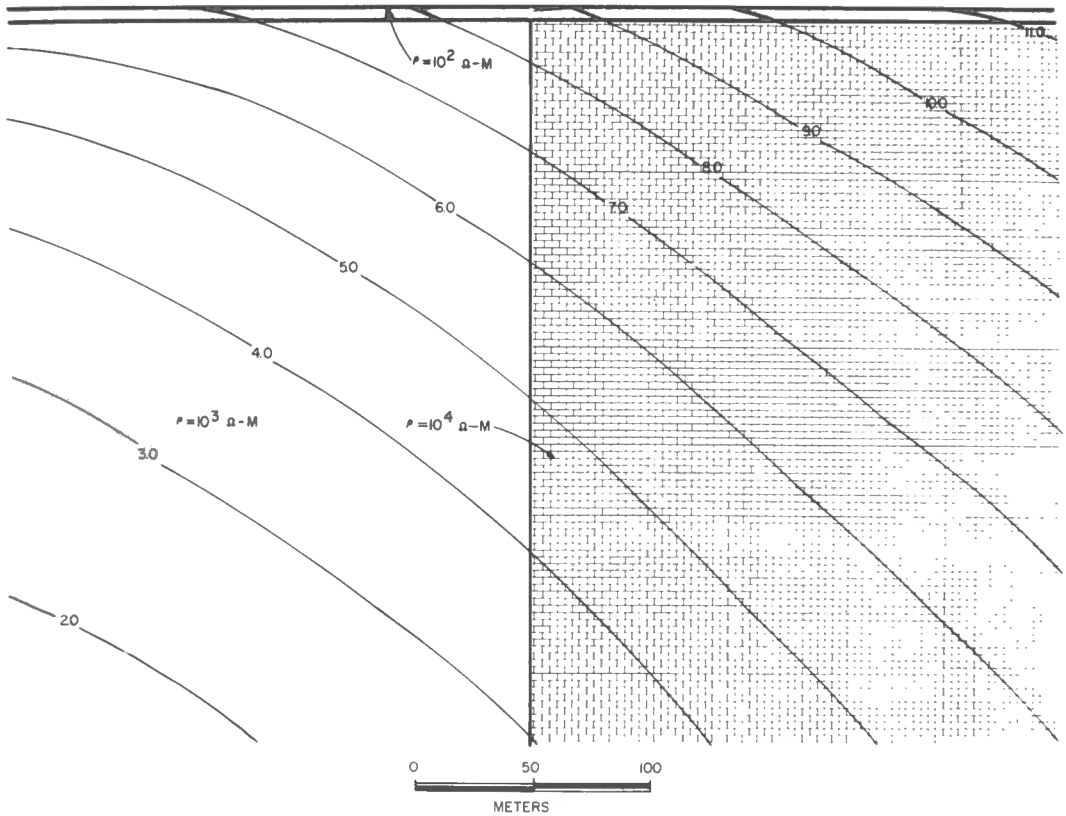

Figure 2.

Subsurface current flow (E_y, relative amplitude distribution) at 10 kHz in the structure of Figure 1.

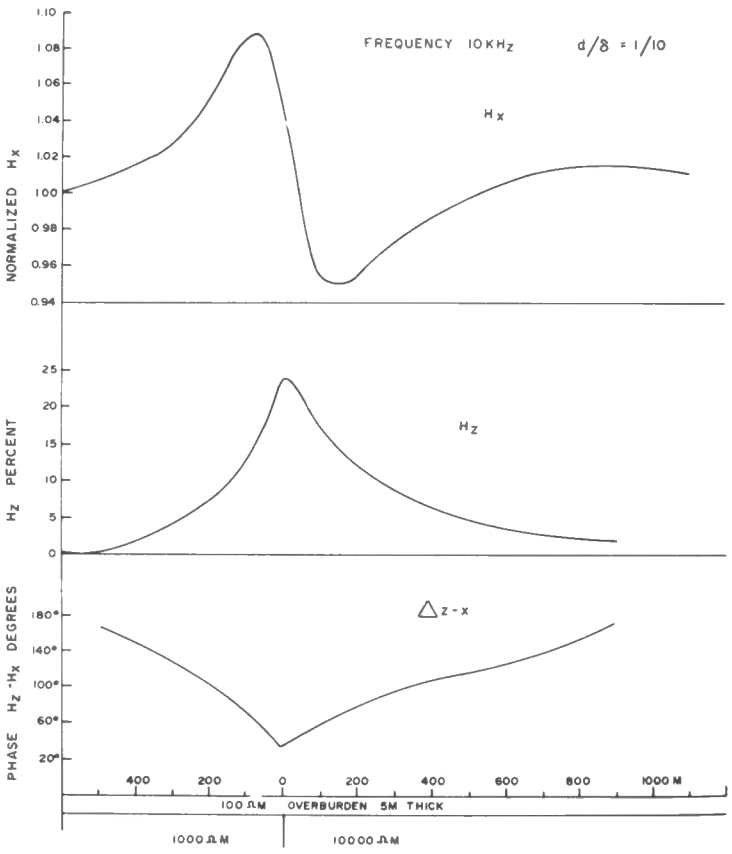

Figure 3. Theoretical profiles of H_x, H_z and Δz-x over structure of Figure 2.

THEORY

Vertical magnetic field variations

A number of authors (Jones and Price, 1970), Swift (1971) have discussed the mathematical basis for the distortion of an electromagnetic plane wave over a vertical discontinuity separating two half-spaces of different conductivity, with and without an overburden layer above. For a remote natural EM source the direction of E, the electrical and H, the magnetic horizontal vectors is random with respect to the co-ordinate system shown in Figure 1. These vectors, however, may be resolved into components parallel and normal to the contact. The appropriate Maxwell equations thus become:

$$\frac{\partial E_z}{\partial x} - \frac{\partial E_x}{\partial z} = j\omega\mu_o H_y$$

$$\frac{\partial H_y}{\partial z} = -\sigma E_x$$

for E normal to strike (H polarization)

and:

$$\frac{\partial H_y}{\partial x} = \sigma E_z$$

$$\frac{\partial E_y}{\partial x} = -j\omega\mu_o H_z$$

$$\frac{\partial E_y}{\partial z} = j\omega\mu_o H_x$$

for E parallel to strike (E polarization)

$$\frac{\partial H_x}{\partial z} - \frac{\partial H_z}{\partial x} = \sigma E_y$$

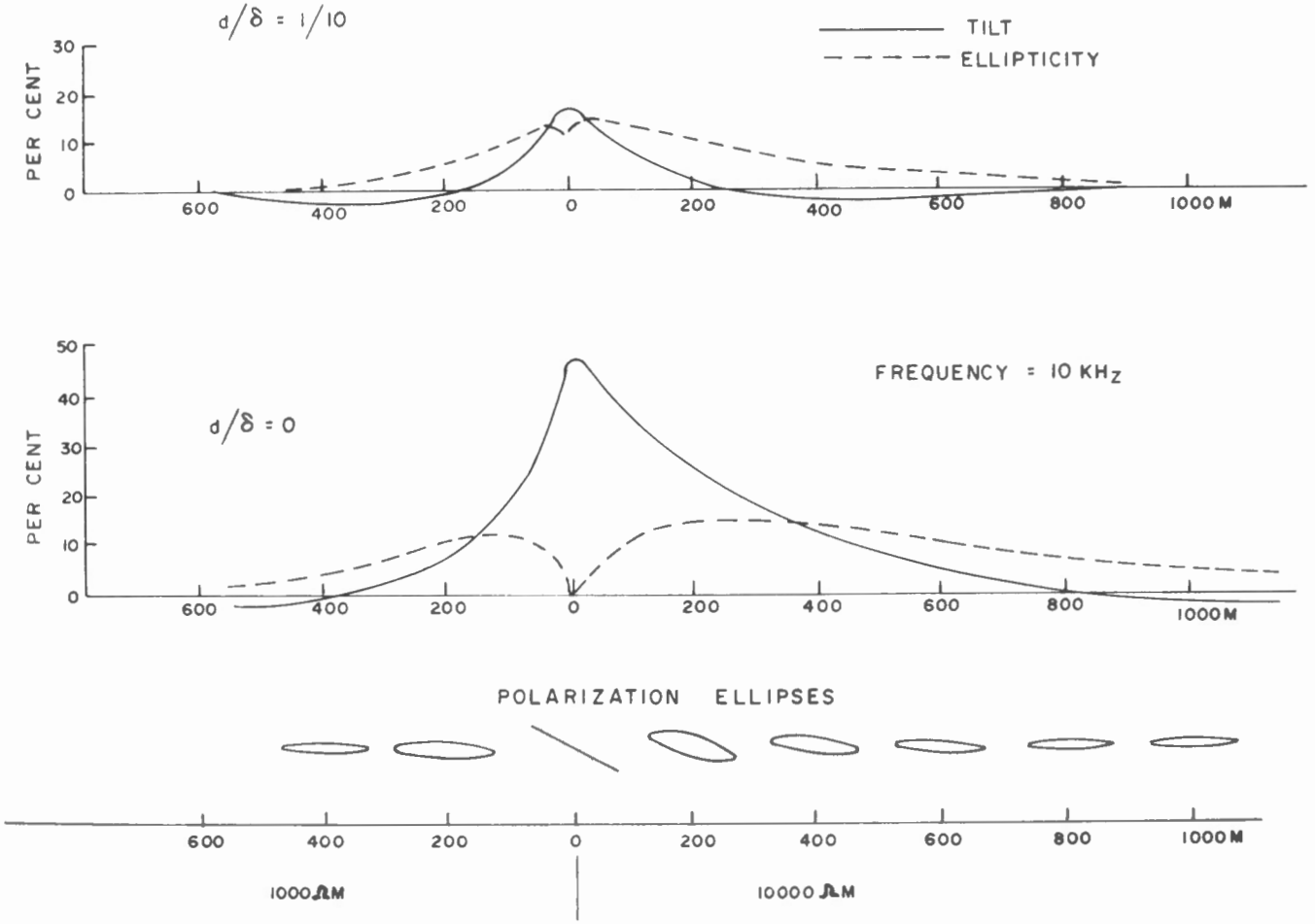

Figure 4. Tilt and ellipticity profiles for $d/\delta = 1/10,\ 0$ for the structure of Figure 2.

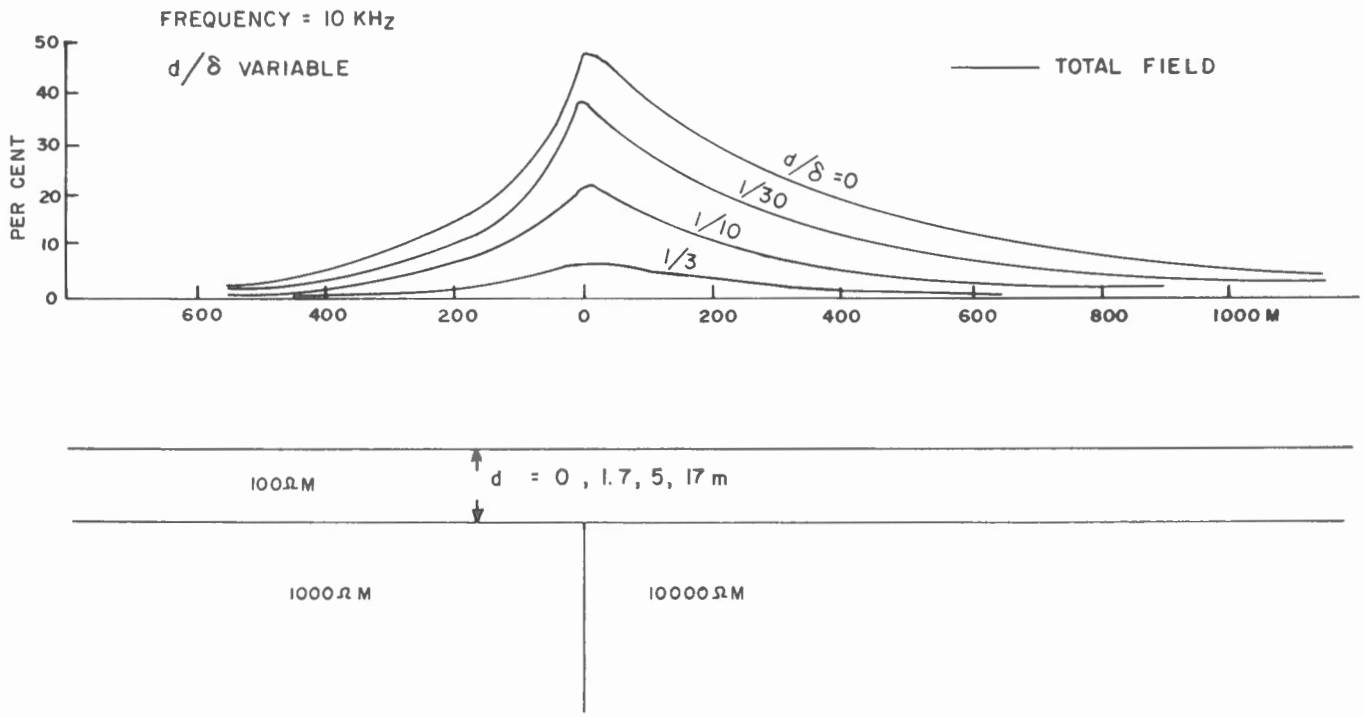

Figure 5. Total field, $|H_z/H_x|$, profiles over the structure of Figure 2 with $d/\delta = 0,\ 1/30,\ 1/10,\ 1/3$.

The E polarization is particularly convenient for the VLF method, which measures H_Z and H_X. It is customary, where possible, to select a remote station whose H_X vector is roughly parallel to the survey lines, that is, the station location is more or less parallel to strike.

The VLF source field, propagating parallel to the earth surface and refracted vertically downward at the ground interface, thus provides H_X and E_Y components approximately in the appropriate direction. The ground current flow may be readily illustrated by calculating with the aid of numerical techniques (Swift, 1967; Madden and Swift, 1969; Ku *et al.*, 1973) the actual subsurface electric field distribution for a given geological situation.

Figure 2 shows the subsurface current flow (actually the E_Y field amplitude distribution) at 10 kHz in the structure of Figure 1 with an overburden of 100 Ωm, 5 m thick and the contact separating beds of 1000 and 10 000 Ωm. Since the skin depth ($\delta = 500\sqrt{\rho/f}$) for 100 Ωm and 10 kHz is about 50 m, the EM wave is not greatly attenuated in the overburden. Use is made of the ratio d/δ, where d is overburden thickness, since it involves all the significant overburden parameters.

Theoretical profiles of H_X, H_Z and Δ_{Z-X} over the same structure, are illustrated in Figure 3. As the fault is approached from the left (conductive side) the horizontal magnetic field increases to a maximum, falls sharply to a minimum as the contact is crossed and then increases slowly to background value as the traverse proceeds to the right. The slope is always steeper on the conductive side of the contact, although increasing overburden thickness and/or conductivity reduces the profile amplitude considerably. For very small values of d/δ the background value of H_X is actually larger on the conductive side than at large distances to the right.

The H_Z field shows a peak directly over the contact which decays to zero on the flanks. Again the slope is steeper on the conductive side and the peak amplitude is controlled by d/δ. In the bottom profile, the phase variation, Δ, between H_Z and H_X is roughly an inverted image of the vertical magnetic field, with a minimum of 32° above the contact and a more or less linear increase on both sides, the steep slope again appearing over the conductive bed. When $d/\delta = 0$ the phase shift is zero

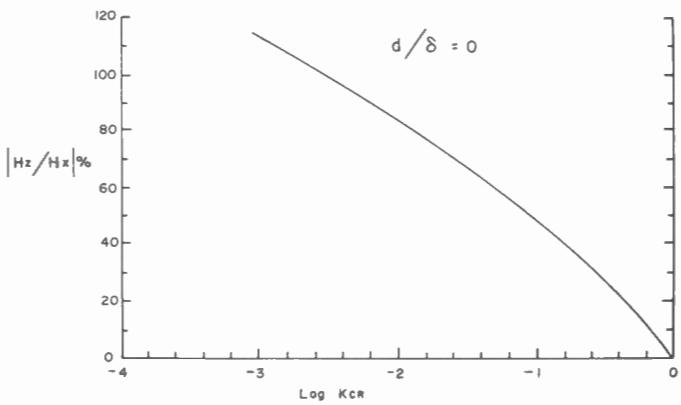

Figure 6. Peak amplitude of total field plotted against log K_{CR} for structure of Figure 2. No overburden.

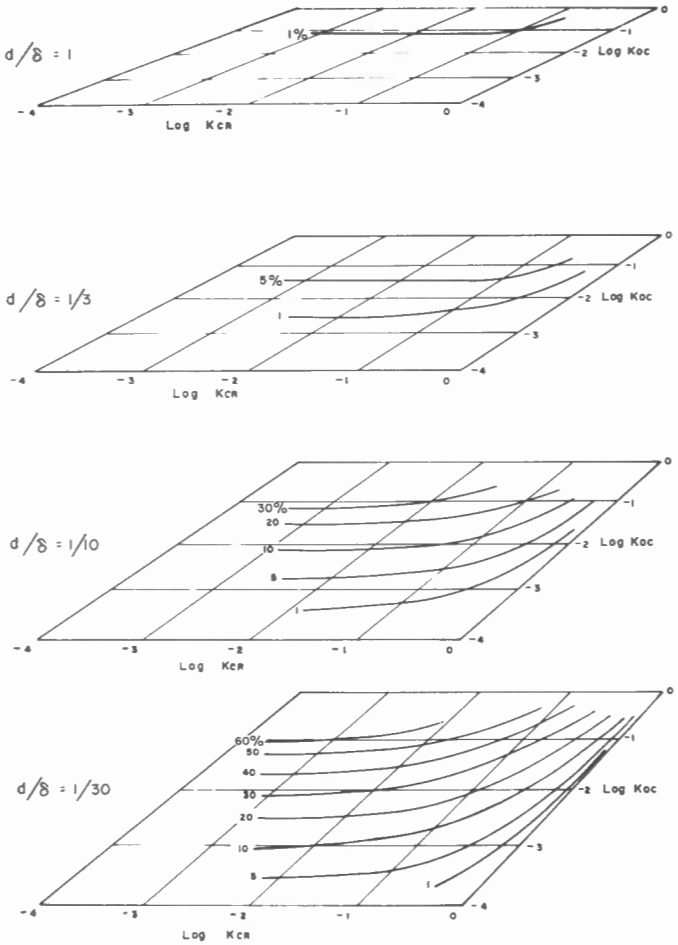

Figure 7. Peak amplitude of total field plotted against log K_{CR} and log K_{OC}, for d/δ = 1, 1/3, 1/10, 1/30 and structure of Figure 2.

at the contact; as this ratio increases, the cusp persists, although its phase increases.

Because H_Z and H_X differ in phase in the vicinity of a conductive discontinuity, the resultant EM wave is elliptically polarized (Heiland, 1940; King, 1971; Paterson and Ronka, 1971). The wave tilt θ (inclination of the major axis with respect to the horizontal) and ellipticity r (ratio of minor to major axes) of the ellipse are given by:

$$\tan 2\theta = \frac{2R\cos\Delta}{1-R^2}$$

$$r^2 = \frac{1+R^2-\sqrt{(1+R^2)^2-4R^2\sin^2\Delta}}{1+R^2+\sqrt{(1+R^2)-4R^2\sin^2\Delta}}$$

where $\Delta = \phi_Z - \phi_X$ the phase difference between vertical and horizontal field components, and, $R = |H_Z/H_X|$ is their amplitude ratio. With a little manipulation and assuming that H_X is considerably larger than H_Z, which is generally the case, these relations become:

$$\tan\theta = R\cos\Delta$$

$$r = R\sin\Delta.$$

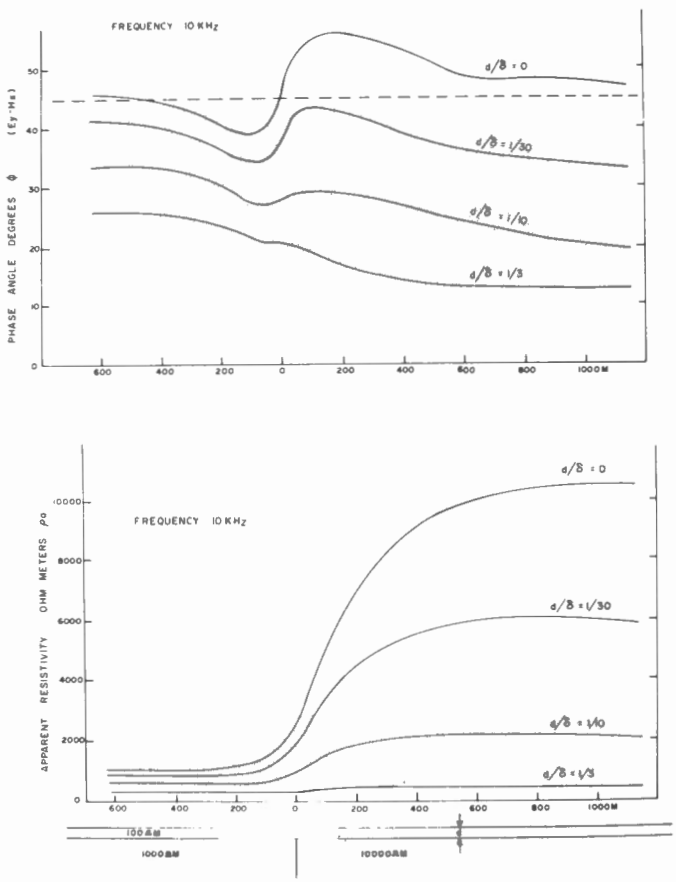

Figure 8. Theoretical profiles of ρ_a and ϕ over structure of Figure 2 for d/δ = 0, 1/30, 1/10, 1/3.

In this case it is useful to note that the total normalized vertical field can be directly calculated from the measurements from:

$$R^2 = \tan^2 \theta + r^2$$

The parameters θ and r are related to "in-phase" and "quadrature" components of the secondary magnetic field (*see* section on instrumentation). Profiles of tilt and ellipticity, for $d/\delta = 1/10$ and zero (no overburden) are shown in Figure 4. The polarization ellipses at several stations along the traverse are included in the latter profile. Directly above the contact, if the value of Δ is zero, the ellipse degenerates to a straight line whose slope is H_Z/H_X.

Clearly the overburden has a pronounced effect on both the tilt and ellipticity profiles. Figure 5 illustrates this point further, where the total vertical secondary field H_Z, expressed as a percentage of the primary field, is plotted for increasing values of d/δ.

Two additional parameters may be employed to determine maximum response over the contact. These are K_{CR}, the ratio of resistivities in the conductive and resistive beds and K_{OC}, the ratio of overburden resistivity to the resistivity of the more conductive bed. When $d/\delta = 0$, the maximum total field response is controlled by K_{CR} only; this is shown in Figure 6, where $|H_Z/H_X|$ max is plotted against log K_{CR}. Figure 7 displays total field values for variable K_{OC} as well as K_{CR}, corresponding to d/δ ratios of 1/30, 1/10, 1/3 and 1. When $d/\delta = 0$, the peak response will be 50% for any K_{CR} = 1/10 (10 Ωm vs 100 Ωm, 1000 Ωm vs 10 000 Ωm, etc.); it should be noted, however, that the profile widths will be different. This will also be true for other values of d/δ when K_{CR} and K_{OC} are fixed.

From the foregoing discussion it is clear that, in areas where the overburden resistivity is large compared to rock resistivity or where $d \approx 0$, it would be possible to use the H_Z measurements to determine the structure parameters from the $|H_Z/H_X|$ max ratio, from the skewness of the profile, and from the profile width. A conductive overburden, however, affects these quantities greatly and other techniques are required. In general, we may summarize the behaviour of EM field components over a vertical fault as follows:

1. The total field response is an asymmetric peak over the fault and decays more rapidly on the more conductive side.
2. The in-phase component of the secondary vertical magnetic field is also an asymmetric peak above the fault and decays more rapidly on the more conductive side.

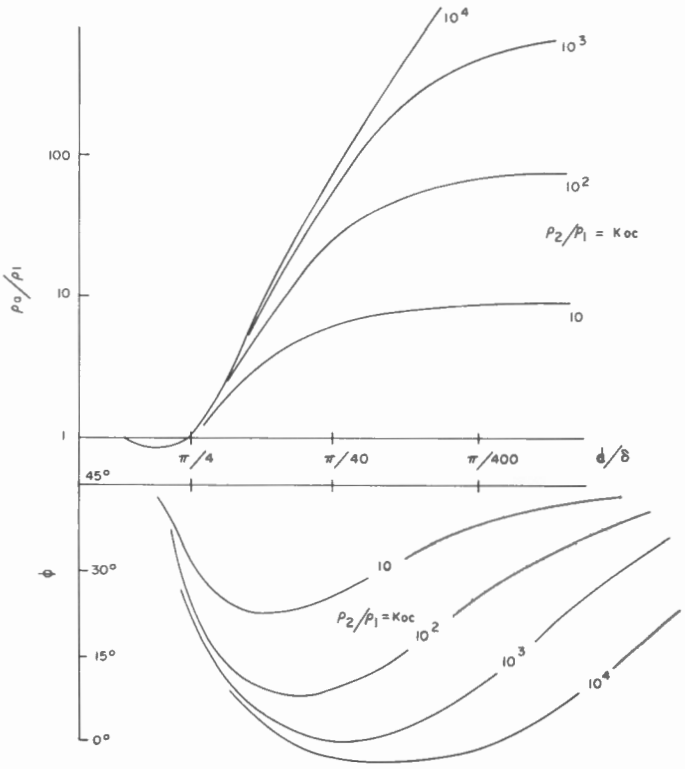

Figure 9. Variations of amplitude $|\rho_a/\rho_1|$ and phase ϕ for two-layer earth with resistive basement (after Cagniard (1953)).

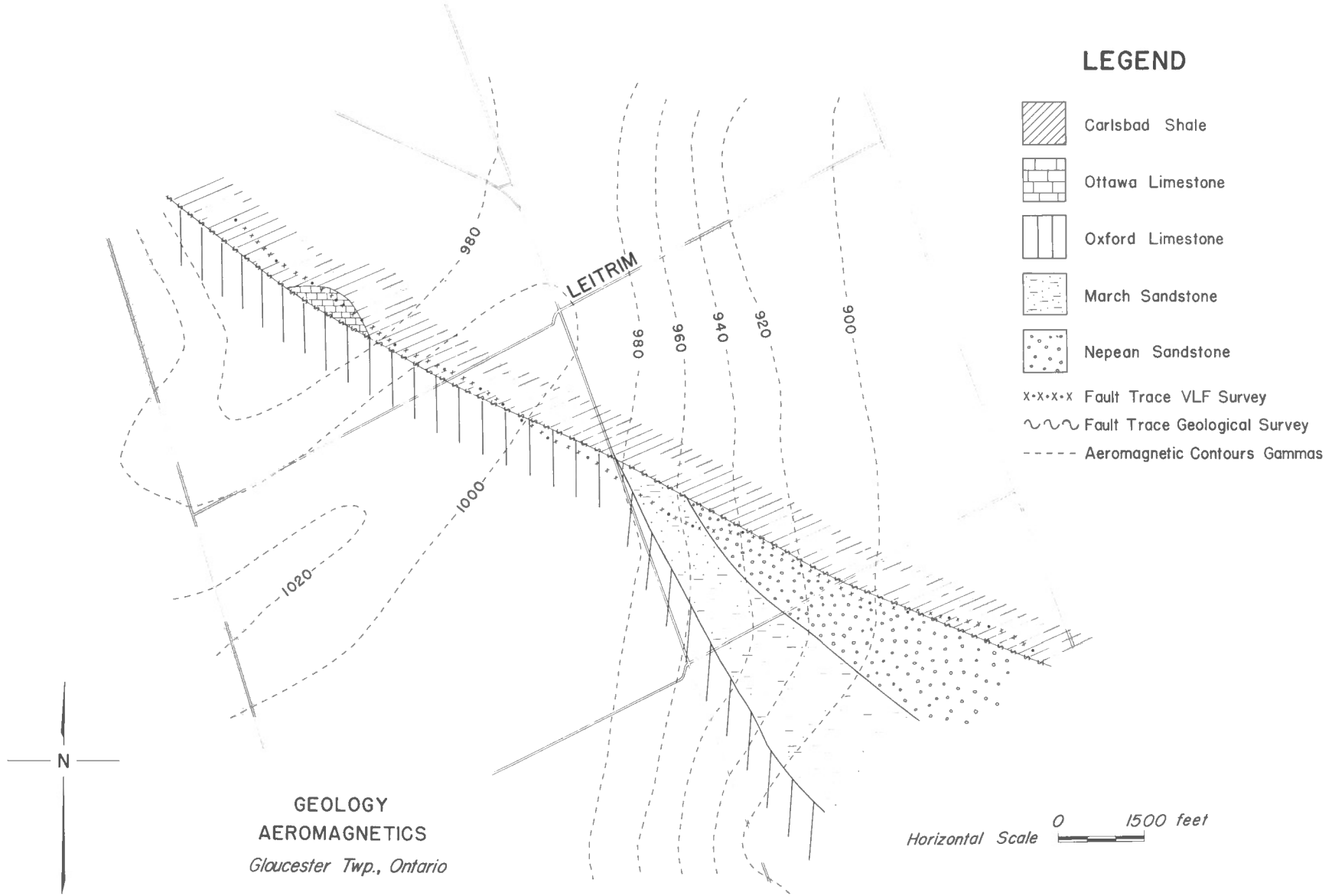

Figure 10. Geology and aeromagnetic contours, Leitrim area.

3. The quadrature component displays a local minimum over the fault, the response being broader than that of the in-phase. The minimum becomes less pronounced with increasing depth of overburden.

4. Both in-phase and quadrature response decrease with increasing depth of overburden. The quadrature response becomes greater than that of the in-phase when the overburden thickness is more than approximately one-half a skin depth.

5. In-phase and quadrature response increase with increasing resistivity contrast across the fault.

6. Anomaly width decreases with increasing frequency, for a given resistivity contrast.

Surface impedance variations

Another method which can be useful for the mapping of lateral discontinuities involves the simultaneous measurement of E_y and H_x as in magnetotellurics (Collett and Becker, 1968). The surface impedance, Z, is the ratio of these two quantities and defines the "apparent resistivity" for the underlying terrain via

$$\rho_a = \frac{1}{\mu\omega} |Z|^2 \qquad \text{in MKS units.}$$

Usually, Z is a complex quantity because E_y and H_x are not in phase with each other. Thus Figure 8 shows theoretical profiles for the apparent resistivity and the phase difference between E and H across the original contact of Figures 2 to 6 for the d/δ ratios used previously. It is again apparent that increasing depth of overburden influences the results by decreasing values of both ρ_a and ϕ on each side of the contact, while smoothing the profile slope directly over it.

Although the variation in the apparent resistivity near the contact can only be calculated numerically, the values of this quantity and the accompanying phase difference, remote from the fault, can be computed analytically. Variations of amplitude $|\rho_a|$ and phase ϕ for a two-layer earth – that is, the overburden layer remote from the fault – are shown in Figure 9. These are the standard master curves developed by Cagniard (1953), reproduced only for a conductive upper layer. Although magnetotelluric sounding normally involves measurement of horizontal orthogonal E and H fields over a range of frequencies, it is possible, by assuming a resistive bedrock, to estimate the overburden parameters from this master chart even when $|\rho_a|$ and ϕ have been determined only at a single frequency in the field.

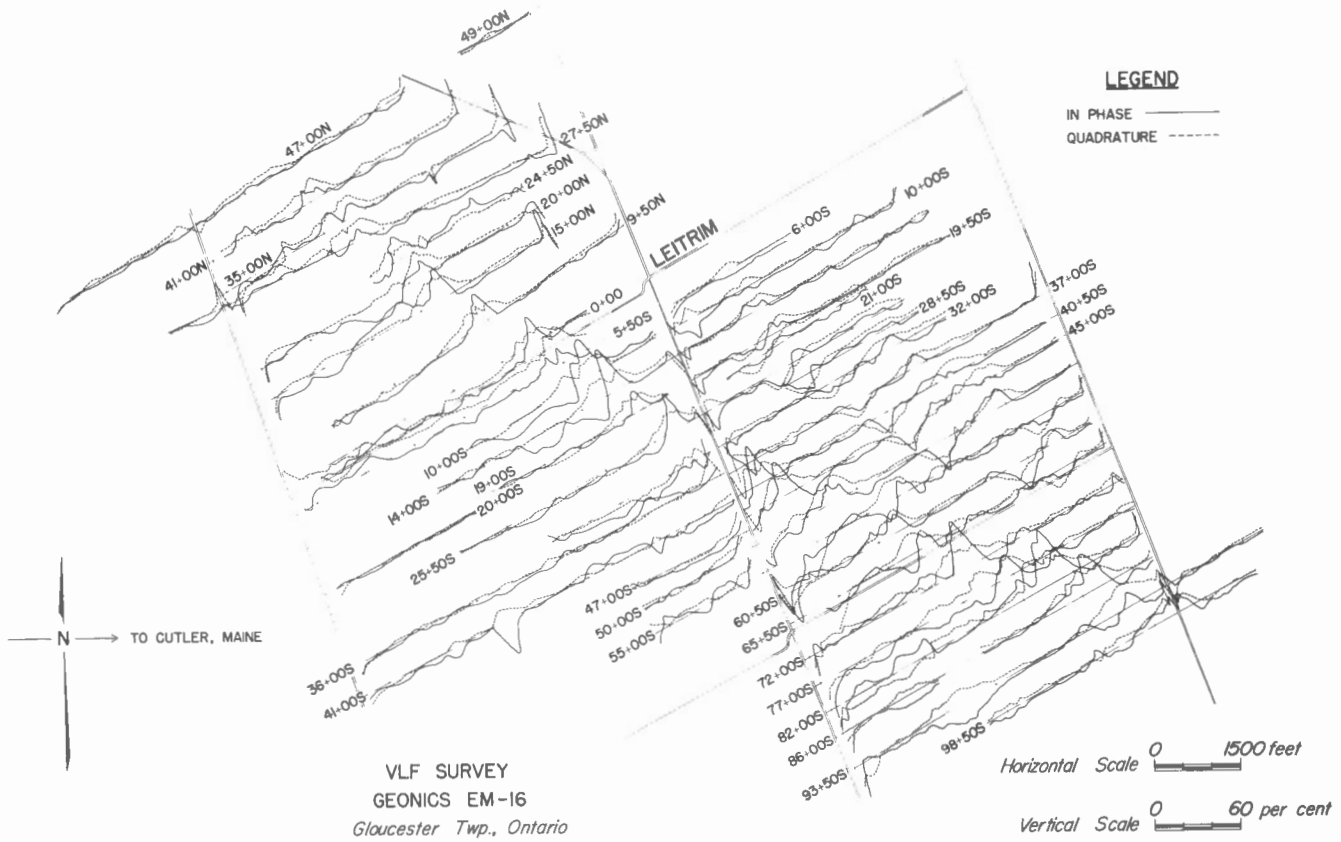

Figure 11. VLF in-phase and quadrature profiles, Leitrim area.

INSTRUMENTATION

Measurement of magnetic field tilt and ellipticity

The Geonics EM16 VLF receiver has been described elsewhere (King, 1971; Paterson and Ronka, 1971; Phillips and Richards, 1975). At least two other instruments – the Scintrex SCOPAS and Crone RADEM – are also designed to measure properties of the polarization ellipse over the same frequency range. With the EM16 a minimum signal is obtained in the receiver by aligning the instrument receiver axes with the major and minor axes of the field polarization ellipse. At this tilt angle, the voltages induced in the two receiver coils are exactly in quadrature with each other and may be directly compared by adding a 90° phase shift to one of them. This comparison is made with the use of the "quadrature" dial which then allows a direct reading of the ellipticity. As indicated previously the tilt angle reading, in percent, is associated with the "in-phase" component of the secondary vertical field and the ellipticity is associated with the "quadrature" component of the same quantity.

In order to avoid ambiguity in profile plotting and interpretation, some sign convention must be maintained during field surveys. From the equations for E-polarization involving H_z and H_x in the previous section, we find that:

$$\frac{H_z}{H_x} = -\frac{\partial E_y/\partial x}{\partial E_y/\partial z}$$

Thus the value of tan θ may be positive or negative, depending on the sign of $\partial E_y/\partial x$; since E_y is larger on the resistive side of the fault, the x-gradient will be positive if the traverse proceeds from the conductive side and vice versa. For consistency the following azimuth orientation was maintained during field work.

For traverses approximately east-west (north-south), the operator faces east (north) as nearly as possible, depending on the transmitter azimuth, to make measurements, while dip angles to the east (north) are reckoned positive. With this convention, both in-phase and quadrature values are positive when the resistive bed lies to the west (south) for an east-west (north-south) traverse, while a negative response indicates the resistive bed is east (north).

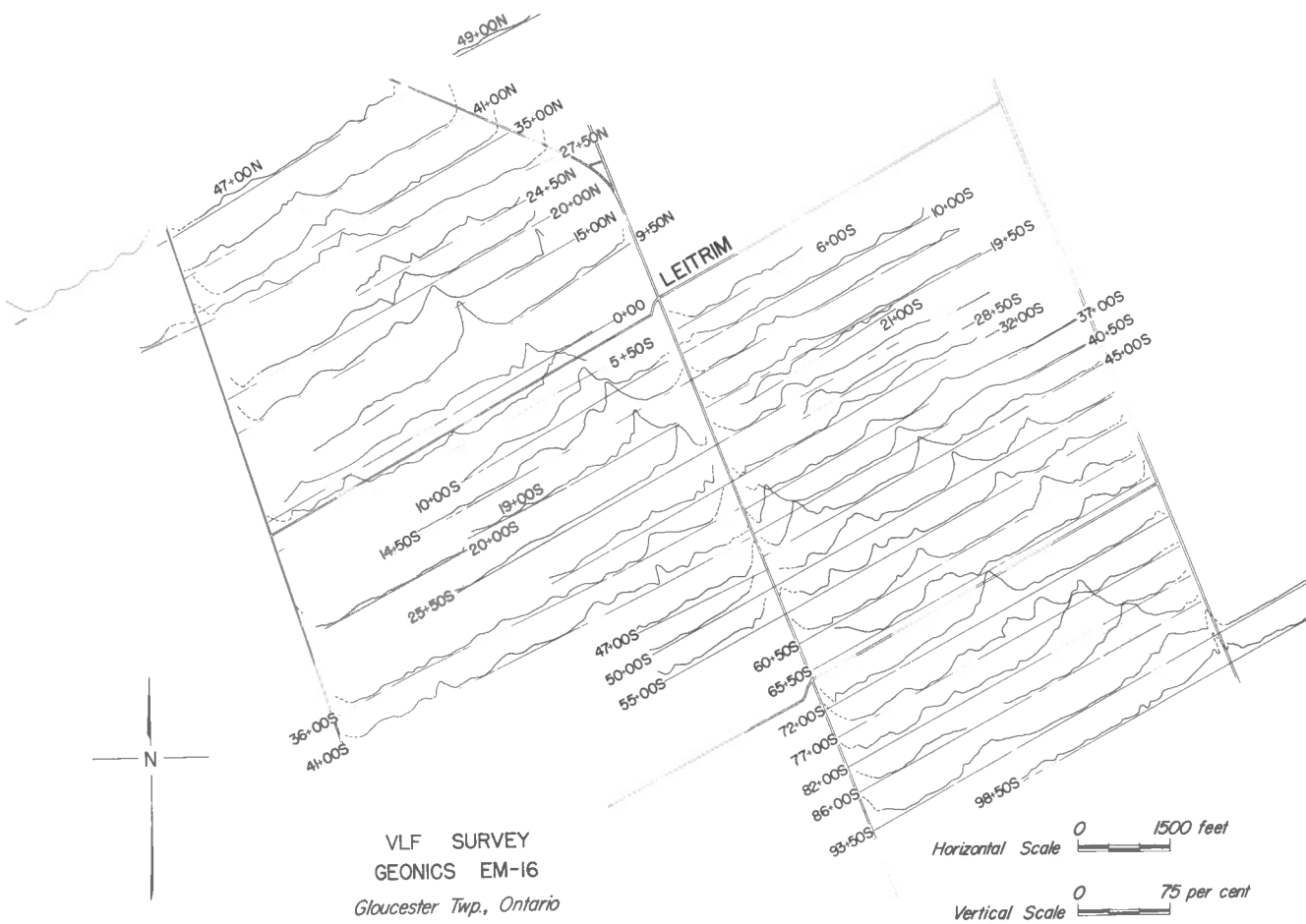

Figure 12. VLF total field profiles, Leitrim area.

Measurement of complex wave impedance

The Westinghouse Georesearch Model C-602 VLF Wave Impedance Meter was used for measuring ρ_a and ϕ. A Geonics EM16R unit, unavailable at the time, is equally suitable for this purpose. Both employ the magnetotelluric method, with a horizontal axis coil to detect the H_x magnetic field component and a 10 m dipole, consisting of two electrodes driven into the ground, for the E_y orthogonal electric field. Both are null instruments. With the Westinghouse meter the ρ_a and ϕ values are read off graphs supplied with the instrument. Its frequency range is 10-60 kHz. The EM16R is a modified form of the EM16, whose frequency range is about 15-25 kHz; resistivity and phase readings are obtained from dial readings at null signal.

FIELD WORK

Gloucester Fault

The principal test area for field work was in the vicinity of Leitrim, near Ottawa, where the Gloucester fault strikes roughly southeast for some 30 miles. The map in Figure 10 includes some geology and aeromagnetic contours. Beds of Carlsbad shale form the north side of the contact, adjoining Oxford limestones in the northwest half, while March and Nepean sandstones occupy the southeast portion (Wilson, 1946).

Aeromagnetic contours indicate very little susceptibility contrast between these formations. The fault trace determined by geological mapping is a smooth line; that outlined by the VLF Survey differs only in detail in some areas. This is a nearly vertical dip-slip fault downthrown to the northeast and displaced upwards on the southwest.

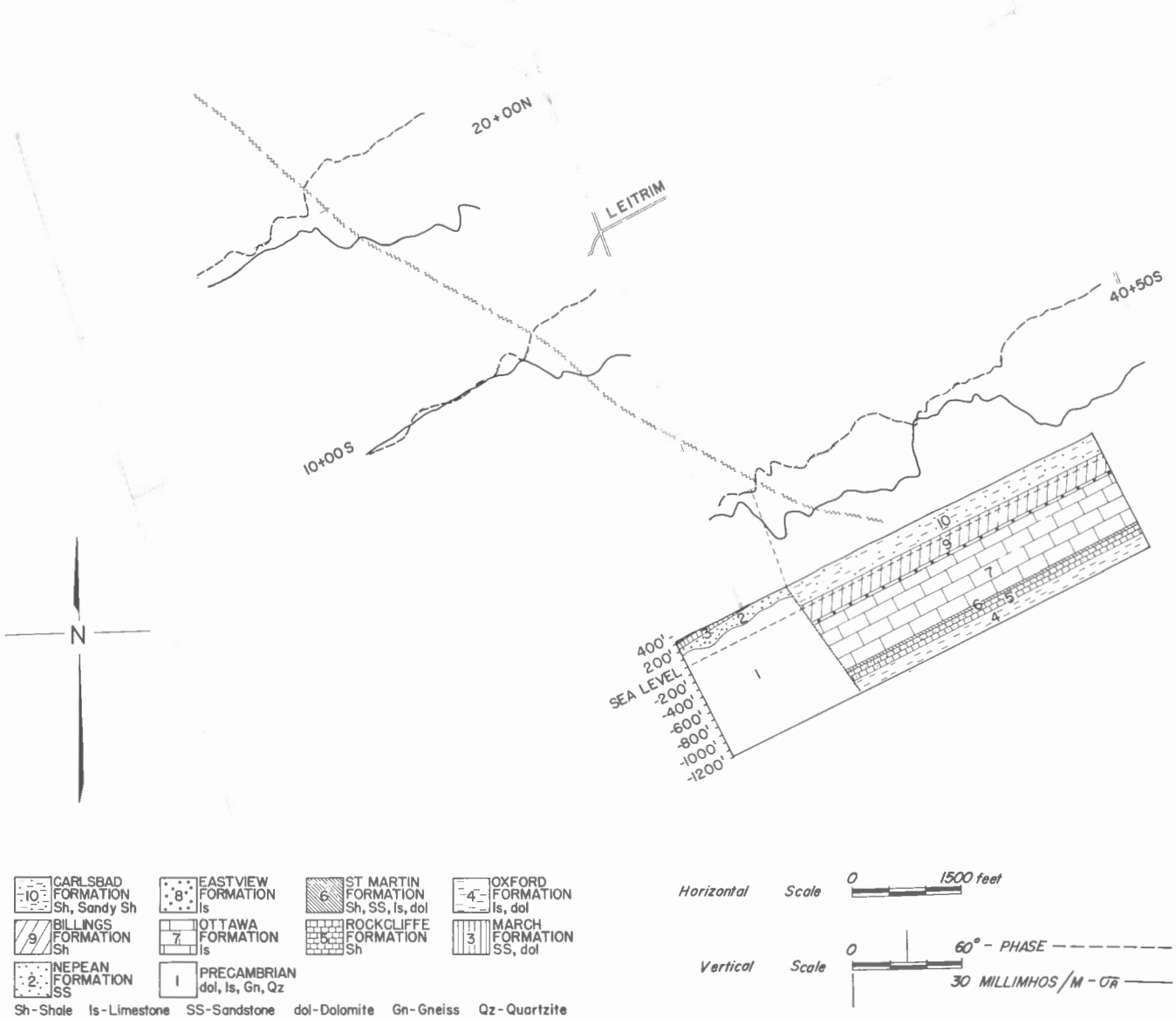

Figure 13. Apparent conductivity (σ_a) and phase (ϕ) profiles on lines 20+00N, 10+00S, and 40+50S, Leitrim area.

A brief description of the various formations and their resistivity is tabulated below (Andrieux written comm., 1971):

Formation	Geology	Resistivity
Carlsbad	Shale, limestone-dolomite	85 Ωm
March	SS-dolomite layers	–
Nepean	SS-siliceous cemented	1500 – 3000
Ottawa	Limestone, shale-SS layers	2000 – 3000
Oxford	Thick dolomite with some ls	5000
Rockcliffe-St. Martin	Shale + SS levels; ls + sh + dolomite	low?

VLF profiles showing in-phase and quadrature response over this area are displayed in Figure 11 and those for the total field (R) in Figure 12. Line spacing was about 500 feet on average and the traverses, approximately normal to the fault, were generally one mile long. As indicated, the lines strike east-northeast; the Cutler Maine transmitter, NAA (17.8 kHz) which is about 400 miles due east of the area, was used for the entire survey. Although a VLF transmitter located approximately north or south of Ottawa would have been more suitable, the Cutler station provided the best signal for this area. Readings were taken facing north. Station spacing varied from 50 feet near the fault to 200 feet remote from it.

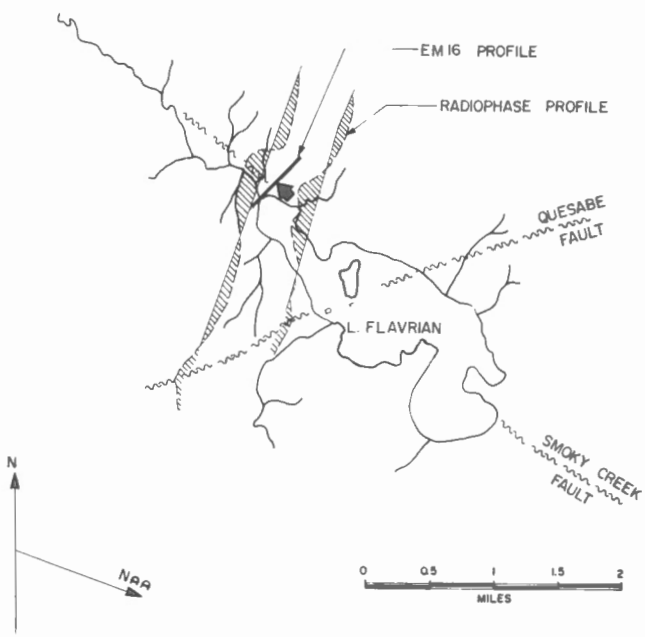

Figure 14. Airborne VLF and traverse line, Smoky Creek fault area, Lake Abitibi-Noranda area.

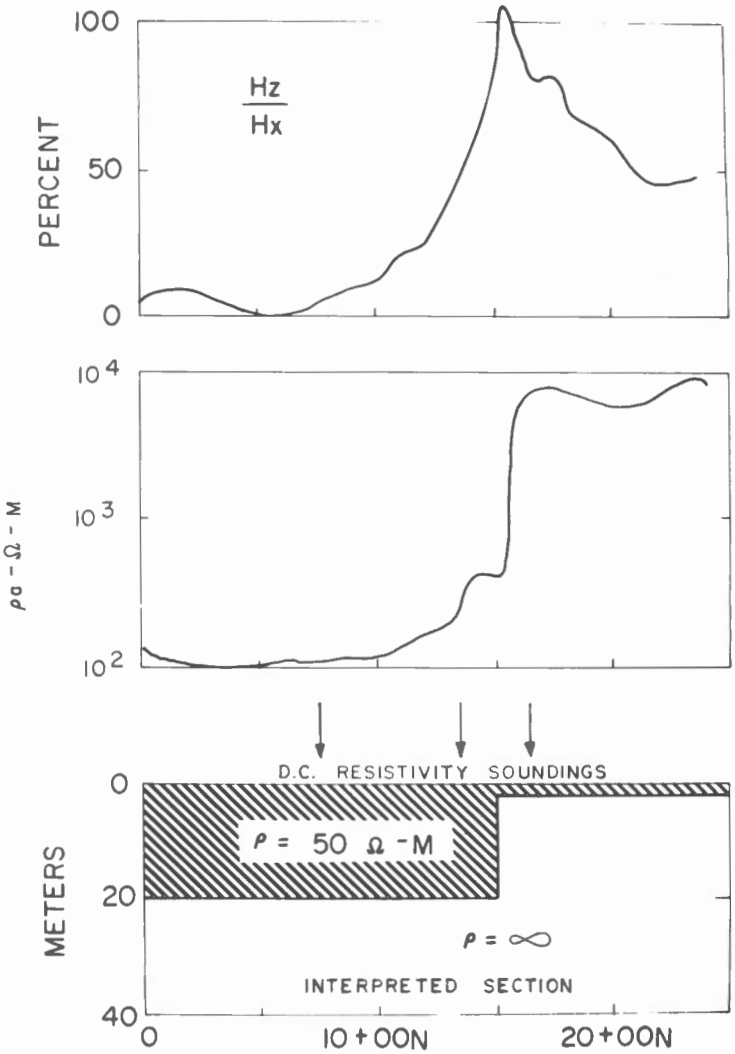

Figure 15. VLF total field, and ρ_a profiles line A3, Smoky Creek fault.

The data displayed in Figure 11 provide excellent examples of the vertical contact between beds of contrasting resistivity. Nearly all the profiles show a pronounced anomaly where the Gloucester fault is expected to occur, consisting of asymmetric in-phase and quadrature peaks with the steeper slope to the northeast, corresponding to the more conductive bed. The quadrature anomalies, which are generally broader, flatter and of smaller amplitude than the in-phase, also have a characteristic local minimum or cusp (e.g. Lines 24+50N, 0+00, 14+00S, 19+00S, 25+50S, 41+00S, 47+00S, 50+00S, 72+00S, 83+00S) coinciding more or less with the in-phase maximum on many profiles.

There is another distinct anomaly about 2000 feet east of the Gloucester fault between lines 21+00S and 65+50S. Both in-phase and quadrature peaks are negative, the latter displaced slightly to the west of the in-phase on several lines, notably 60+50S. The steeper slope is on the southwest. Slight quadrature cusps are evident on lines 40+50S, 45+00S and 50+00S. These data define a second contact with the resistive bed to the northeast.

A third anomaly still farther east appears between lines 32+00S and 60+50S. Here the peaks are positive and the asymmetry indicates the resistive bed is on the southwest side of the contact. The quadrature response is larger than the in-phase on several lines. This feature, which is about 1300 feet east of the second contact on line 32+00S, appears to merge with it to the southeast. On line 60+50S the separation has decreased to about 800 feet, producing a crossover type of response due to the proximity of the positive and negative peaks.

The total field profiles of Figure 12, although they contain less information than Figure 11, probably give a clearer picture of the three contacts discussed above, since the anomalies are all positive and there is less clutter.

Wave impedance profiles carried out on lines 20+00N, 10+00S and 40+50S are shown in Figure 13. Here we have plotted the apparent conductivity (reciprocal of apparent resistivity) and ϕ the phase difference from 45°. On line 20+00N there is one pronounced break for both parameters, approximately at 36+00W. The generally low apparent conductivity 4 – 2 millimhos/m west of this station rises sharply and remains greater than 20 millimhos per metre for the eastern portion of the traverse. The phase angle between E_y and H_x increases abruptly at the same point and there is a difference of 15° – 20° between the average values either side of it. These results agree qualitatively with the theoretical profiles of Figure 8, that is, the more conductive bed on the east produces a larger phase angle than on the resistive side, unless the structure outcrops. In this case the fact that the phase angle on the conductive side exceeds 45° seems to indicate the presence of a resistive overburden on that side.

The profile from 10+00S exhibits the same properties as the one from 20+00N, the contact being at 15+00W. Although the phase break is not as pronounced here, the difference between the average values of east and west sections is about 15°. Comparing all four profiles with Figures 11 and 12, it is clear that the fault is located within 50 feet in all cases.

Three contacts are indicated in the σ_a and ϕ profiles for line 40+50S, near stations 6+00E, 29+00E and 44+50E. These results correlate well with EM16 profiles in Figures 11 and 12, where peaks appear at 5+50E, 29+00E and 44+00E, corresponding respectively to the Gloucester and the two additional faults discussed previously. All the previous remarks concerning lines 20N and 10S apply here as well.

It is to be noted that the geological section derived by Wilson (1946), which is also shown in Figure 13, agrees with the position of the fault as indicated by the VLF measurements. It does not, however, suggest the presence of the other two features farther to the east.

Summing up, the correlation between field results and theory is excellent. In particular, there does not appear to be any anomalous conductivity associated with the faults themselves, such as exhibited by graphite and water-filled shear zones. In Figure 12 the trace of the Gloucester fault as mapped by the VLF survey wanders somewhat from its location determined geologically by Wilson (1946). The variation, however, is generally within 500 feet.

The wave impedance measurements located all the contacts within 50 feet of their positions found in the tilt angle survey, which is roughly the error in the pace and compass traverses employed. The apparent conductivities of the Carlsbad and Oxford formations obtained by these measurements, about 15 and 3 millimhos/m respectively, do not represent true formation resistivities, because of the presence of overburden. The fact that the phase variations, in the vicinity of Gloucester fault, do not agree with the theoretical profiles in detail is probably due to irregularities in the overburden and/or multilayer beds on both sides of the contact.

Detection of the two faults east of the Gloucester fault indicate a resistive zone in the Carlsbad Shale (*see* Fig. 13, line 40+50S between 29+00 and 44+00E) which cannot be due to a change in the bedrock terrain, since both overburden and shale resistivities are comparatively low. The resistive block may be Ottawa limestone, locally uplifted from below the Carlsbad; outcrops of this formation are found northwest of Leitrim.

Smoky Creek Fault

Further field tests were carried out over the Smoky Creek fault in the vicinity of Lake Flavrian, several miles northwest of Noranda, Quebec. The fault strikes southeast for about 20 miles in the area. The geological map for the area indicates granodiorite on both sides, that is, there is no contrast in lithology across the contact. This feature was indicated by an early airborne AFMAG survey (Sutherland, 1967) and more recently by an airborne VLF Barringer RADIOPHASE survey (Becker and McNeil, 1969). The field situation is shown in Figure 14 which indicates the position of one VLF profile (line A3) with respect to the fault and the airborne anomalies.

EM16 total field profiles, together with the corresponding apparent resistivity profile are shown in Figure 15 for line A3. Here, the Smoky Creek fault is located at station 15+50N, marked by extremely high (100%) total field peak and a very abrupt increase in resistivity from 100 Ωm to 6000 Ωm. The steep slope of the EM16 profiles is also consistent with the more conductive zone on the south side.

DC resistivity shallow depth soundings were carried out in an attempt to clarify the EM16 results. These indicate that the thickness of the overburden is at least 57 feet at 7+50N, 43 feet at 13+50N, but 6 feet or less at 16+50N. This abrupt change in depth of a conductive (< 100 Ωm) layer – essentially a steep contact between overburden and resistive bedrock – is the source of the anomaly. Possibly the fault itself, supposedly located at 15+50N, is responsible for the bedrock step, although there is no evidence to support this. Thus the VLF and ρ_a profiles, although characteristic of a contact between two beds of different resistivity, appear to be the reflection of a sudden change in the depth of overburden.

CONCLUSION

The field results described in this report agree very well with the theory of VLF response over a vertical contact between beds of contrasting resistivity, covered by a uniform layer of overburden. Thus the method is a useful qualitative supplement to field geology in mapping such structures. Subsequent work in the Ottawa Valley and St. Lawrence Lowlands (Williams, 1976) has confirmed this.

In areas where there are abrupt changes in depth of overburden, however, the VLF data may be misleading, as described in the survey of the Smoky Creek fault. Similar sudden lateral changes in overburden resistivity, although no examples are given here, would doubtless have the same effect. At present shallow seismic and resistivity sounding are the only geophysical methods available to clarify such situations: both are slow and relatively expensive. Obviously a simple and rapid technique for mapping bedrock terrain and estimating overburden resistivity is very desirable, not only in connection with the type of survey described here, but in many other applications as well.

REFERENCES

Becker, A.
1967: Radio-wave mapping of ground conductivity anomalies; *in* Report of Activities, Part A; Geol. Surv. Can., Paper 67-1A, p. 130-131.

Becker, A. and McNeil, J.D.
1969: Explanatory notes, Noranda Radiophase Survey; Published by Quebec Department of Natural Resources.

Cagniard, L.
1953: Basic theory of the magneto-telluric method of geophysical prospecting; Geophysics, v. 18, p. 605-635.

Collett, L.S. and Becker, A.
1968: "Radiohm Method for Earth Resistivity Mapping"; Canadian Patent No. 795, 919.

Collett, L.S. and Bell, C.K.
1971: AFMAG use in geological interpretation; Can. Min. Metall. Bull., v. 64, p. 39-47.

Dosso, H.W.
1966: Analogue model measurements for electromagnetic variations near a coastline; Can. J. Earth Sci., v. 3, p. 917-936.

Fraser, D.C.
1969: Contouring of VLF-EM data; Geophysics, v. 34, no. 6, p. 958-967.

Geyer, R.G.
1972a: Transient electromagnetic response near a fault zone; Geophys. Prospect., v. 20, p. 829-846.

1972b: The effect of dipping contact on the behaviour of the electromagnetic field; Geophysics, v. 37, p. 337-350.

Heiland, C.A.
1940: Geophysical Prospecting, chap. 10, Prentice-Hall, New York.

Jones, F.W. and Price, A.T.
1970: Perturbations of alternating geomagnetic fields by conductivity anomalies; Geophysc. J. R. Astron. Soc., v. 20, p. 317-334.

King, W.F.
1971: Studies of geologic structures with the VLF method; unpubl. M.Sc. thesis, McGill Univ., Montreal.

Ku, C.C., Hsieh, M.S., and Lim, S.H.
1973: The topographic effect in electromagnetic fields; Can. J. Earth Sci., v. 10, p. 645-656.

Madden, T.R. and Swift, C.M., Jr.
1969: Magneto-telluric studies of the electrical conductivity structure of the Crust and Upper Mantle; *in* The Earth's Crust and Upper Mantle; Geophysc. Monograph. 13, (ed. P.J. Hart), p. 469-479; Am. Geophys. U., Washington, D.C.

Paterson, N.R. and Ronka, V.
1971: Five years of surveying with the VLF EM Method; Geoexploration, v. 9, p. 7-26.

Phillips, W.J. and Richards, W.E.
1975: A study of the effectiveness of the VLF Method for the location of narrow-mineralized fault zones; Geoexploration, v. 13, p. 215-226.

Sutherland, D.B.
1967: AFMAG for EM mapping; *in* Mining and Groundwater Geophys.; (ed. L.W. Morley), Geol. Surv. Can., Econ. Geol. Rep. 26, p. 228-237.

Swift, C.M., Jr.
1967: A Magneto-telluric investigation of an electrical conductivity anomaly in the Southwestern United States; unpubl. Ph.D. thesis, M.I.T., Cambridge, Mass.

1971: Theoretical magneto-telluric and Turam Response from 2-dimensional inhomogeneities. Geophysics, v. 36, p. 38-52.

Weaver, J. T.
1963: The electromagnetic field within a discontinuous conductor with reference to geomagnetic micropulsations near a coastline; Can. J. Phys. v. 41, p. 484-495.

Williams, D. A.
1976: A study of the fault systems in the St. Lawrence Lowlands and Ottawa Valley areas; Ph. D. thesis, McGill Univ., Montreal. (in prep.)

Wilson, A. E.
1946: Geology of the Ottawa-St. Lawrence Lowlands, Ontario and Quebec; Geol. Surv. Can., Mem. 241.